SEPTEMBER 1991 LIDS-P-2066

APPLICATION OF MULTIVARIABLE DESIGN TECHNIQUES TO ROBUST CONTROL OF A LARGE-SCALE SYSTEMS

by

Kelly D. Hammett, John R. Dowdle, Michael Athans

and Karl W. Flueckiger

AIAA-91-2833-CP

APPLICATION OF MULTIVARIABLE DESIGN TECHNIQUES TO ROBUST CONTROL OF A LARGE-SCALE SYSTEM*

Kelly D. Hammett **, John R. Dowdle†, Michael Athans‡, and Karl W. Flueckiger£

The Charles Stark Draper Laboratory, Inc.
555 Technology Square
Cambridge, MA 02139

Abstract

Typical issues and tradeoffs resulting from application of various modern multivariable controller design techniques to large-scale systems are illustrated herein by synthesis of robust H_2 optimal, H_∞ optimal, and H_∞ loop-shaped compensators for a space-based laser beam control example problem using reduced-order models. A design framework is adopted which allows stability robustness in the presence of resulting neglected dynamics to be guaranteed via unstructured uncertainty representation and the Small Gain Theorem, and performance robustness to be independently verified. Infinity-norm bounds on two closed-loop transfer functions provide the key figures-of-merit for guaranteeing the desired stability robustness and nominal performance conditions. A final design is obtained which is verified to meet nominal performance specifications, and is also seen to possess robustness of both stability and performance to dynamics truncated in the model reduction process. The effects of open-loop pole parametric uncertainty are also examined, the main result observed being a severe degradation in closed-loop system performance.

1. Introduction

The complexity of large-scale dynamic systems provides a challenging proving ground for modern multivariable control system analysis and design techniques. High plant dimensionality inherent in large-scale systems can lead to breakdowns in numerics of state-space algorithms or intolerably long computational times, necessitating use of model reduction techniques. Reducing plant order consequently introduces unmodeled dynamics into the system, which must then be accounted for via stability and performance robustness considerations. Additionally, parametric errors in the open-loop system model invariably exist, and their effects must be considered. The lightly damped nature of typical large-scale systems is also a design issue of concern, leading to extremely slow oscillatory transient responses, and, due to the location of lightly damped poles near the complex plane imaginary-axis, potential difficulties in obtaining closed-loop stability and/or stability robustness.

This paper addresses several of the above issues in the context of multivariable feedback design for a chosen example problem. The results presented in this paper stem from a continuing research effort focusing on robust control of large-scale systems. Previous research[1] discussed modern multivariable design methodologies, and addressed possible application to primary mirror beam jitter control of a space-based laser (SBL). In a subsequent work[2], H_∞ optimization and reduced-order models were employed to perform requirements analysis for the combined beam jitter and segment phasing aspects of the SBL beam control problem, and preliminary H_2/H_∞ designs were examined. The results given in this paper extend the results of the previous research to include application of loop-shaping design methodologies to obtain a final design which meets specified beam jitter/segment phasing performance objectives, and possesses both stability and performance robustness to modeling errors introduced during the model reduction process. Additionally, the effects of open-loop pole parametric uncertainty on closed-loop stability and performance are investigated. In Section 2 of this paper, details of the SBL analyzed are given. Section 3 describes the application of model reduction techniques, and Section 4 covers the robustness analysis and compensator synthesis methods used for control system design. Section 5 presents results of controller synthesis utilizing various compensator design techniques, comparison of which allows selection of a best design. Section 6 then verifies performance of the chosen compensator design via time-domain simulation with stochastic disturbance inputs. Finally, Section 7 concludes the paper by addressing performance robustness and parametric uncertainty issues.

As mentioned previously, the example problem

* This paper was prepared by the authors under Independent Research and Development funding at The Charles Stark Draper Laboratory, Inc.

** 1 Lt. Kelly Hammett (USAF) is a C.S. Draper Laboratory Fellow, graduate student at the Massachusetts Institute of Technology, Cambridge, MA, and Student Member AIAA.

† John Dowdle is Chief, Flight Systems Section, C.S. Draper Laboratory, Cambridge, MA.

‡ Michael Athans is a Professor of Electrical Engineering, Massachusetts Institute of Technology, Cambridge, MA.

£ Karl Flueckiger is a member of the Technical Staff, C.S. Draper Laboratory, Cambridge, MA.

Copyright © 1991 by the American Institute of Aeronautics and Astronautics, Inc. All rights reserved.

chosen for illustration of design issues is a wide-field-of-view rapid-retargeting space-based laser (SBL) with features typical of large-scale flexible space structures. Before proceeding further, a brief and somewhat general description of an assumed SBL physical system concept and relevant terminology is presented to facilitate discussion.

The envisioned spacecraft includes both the flexible forward body, referred to as the beam expander assembly (BEA, see Figure 1) due to its primary purpose of laser beam pointing and magnification, and the aftbody, which houses the laser generating equipment and satellite attitude control system. While these two major components necessarily interact dynamically, the analysis of the forward body is the most critical due to its structural flexibility and importance to beam control functions, and, therefore, this study addresses only the performance of the beam expander with the structural model "isolated" from the aftbody. The role of the aftbody is limited to imparting two vibrational torque disturbances to the forebody via an imperfect gimbal isolation subsystem, thereby necessitating active feedback control of the BEA optics. A finite element model of the BEA, described in Section 2, was derived to facilitate control system design.

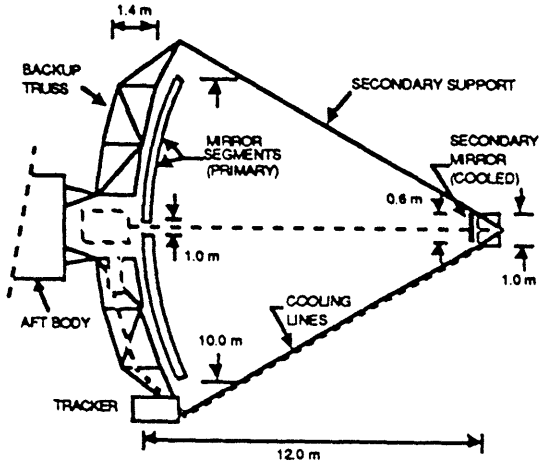

Figure 1. SBL BEA Concept.

2. The SBL Model

The optical design of the SBL beam expander consists of a 10-m diameter paraboloidal primary mirror with a 12-m focal length and a confocal secondary mirror with a 0.8-m focal length and a 0.67-m diameter. Due to deployment and manufacturing limitations, the primary mirror is composed of four segments or petals attached to rigid reaction structure plates (one center and three outer segments, see Figure 2). Each segment reaction structure is in turn kinematically mounted by six segment position actuators to a graphite-epoxy bulkhead truss. The six segment position actuators per petal provide six independent degrees-of-freedom for controlling the rigid body rotation and translation of each primary mirror segment in three orthogonal directions, thereby enabling desired control functions to be accomplished. The secondary mirror is modeled as a rigid body kinematically mounted by control actuators to the tripod metering truss, although the secondary mirror actuators are not employed in this study. The bulkhead and metering trusses are modeled using beam bending elements, and additional lumped masses are included in the finite element model to account for all nonstructural masses, such as the mirror electronics and target tracker.

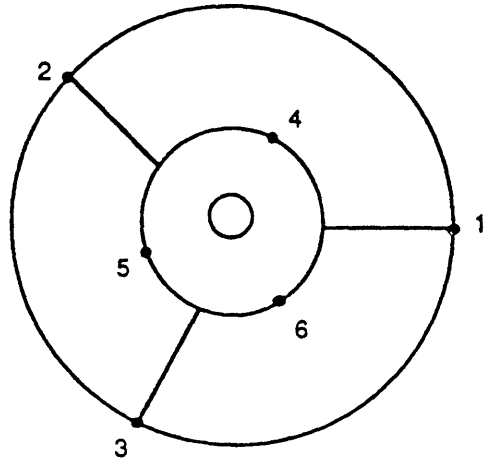

Figure 2. Primary Mirror Segments and Segment Phasing Measurement Locations.

Since the ultimate objective of a space-based laser is to destroy targets by the efficient transfer of energy, optimizing worst-case laser wavefront quality and pointing performance in the presence of the assumed torque disturbances is identified as the primary SBL control system requirement. Therefore, for a given level of disturbance torque (characterized by a bound on its root-mean-square (RMS) value), system performance specifications are identified as minimizing RMS beam deviation from the desired aimpoint (jitter control) and simultaneous minimization of RMS longitudinal separations between primary mirror segment edges (segment phasing). Such segment edge separations induce destructive optical interference, aberrating the laser wavefront, and thereby degrading beam quality. Note that laser beam wavefront aberration due to deformation of the primary mirror segments themselves is not considered in this study. An outgoing wavefront sensor (OWS), collocated with the secondary mirror, measures line-of-sight (LOS) jitter errors in the plane normal to the line of sight, while six segment edge sensors provide information necessary for segment phasing control (reference Figure 2).

Finite element analysis provides a modal model of the system, consisting of 195 structural modes, which in turn is readily transformed into a state-space system representation consisting of 390 states, *i.e.*,

$$\dot{x} = Ax + Br$$

$$y = Cx + Dr$$

where x represents the system's 390 states, y consists of the 2 LOS jitter sensor measurements at the OWS and 6 segment phasing edge gap measurements, and r is a concatenation of the primary mirror's 24 rigid body segment position actuator commands and 2 disturbance inputs creating moments about the base of the mirror. (A damping ratio, ζ, of 0.005 is assumed for all structural modes.) This linear state-space model can be employed in model reduction techniques and modern multivariable linear systems analysis, as illustrated in Sections 3 and 4.

3. Model Reduction

Due to the large dimension of the state-space model developed, reduction of model order is necessary to ease the computational requirements associated with control system design. A thorough and systematic treatment of reduced-order model (ROM) development was published by Moore[3]. The technique proposed by Moore, which is often called balance and truncate (B&T), uses a state-space representation (A,B,C,D) of the plant describing the relationship between the inputs, states, and measurements in which the respective steady-state controllability and observability gramians

$$P = \int_0^\infty \exp(At)\, BB^T \exp(A^T t)\, dt$$

$$Q = \int_0^\infty \exp(A^T t) C^T C \exp(At)\, dt$$

are diagonal and equal. The diagonal elements of the gramians, referred to as Hankel singular values (HSVs), provide the basis for model reduction. Large HSVs correspond to states that are easily controlled and observed, while small HSVs define states that are difficult to control and observe. Thus, the state-space model can be partitioned into strongly and weakly controllable/observable states and the subspace of weakly controllable/observable states may be deleted.

In Figure 3, a plot of absolute modeling error versus ROM order for the SBL BEA model, as measured by the infinity-norm, is given for the B&T method.* A significant knee in this plot is seen at order 12 where all six rigid body mode pairs of the BEA are included in the ROM, and another pronounced knee is found for a ROM of 34 mode pairs (68 states). This suggests that states beyond the 68-state level are not as significant to the system input/output behavior as the first 68 states, and may thus be removed from the system model.

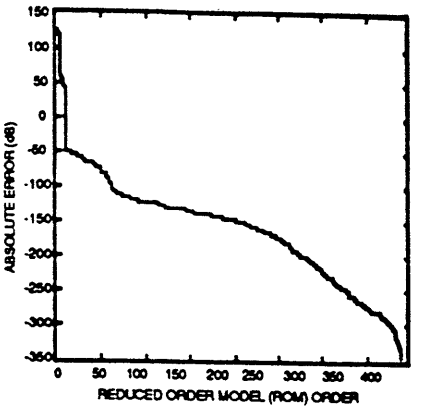

Figure 3. B&T Reduced Order Model Absolute Error.

Additionally, examination of individual observability and controllability gramians from the separate disturbances and actuators reveals that while the six rigid body mode pairs are very observable in the system outputs, they are almost totally uncontrollable from the system segment position actuator inputs. Consequently, rigid body motion of the BEA must be controlled by other actuators, and, therefore, the rigid body modes can be removed from the system model. Doing so yields a 56 state ROM of the BEA for control system design purposes. The maximum singular value bode plots for the full-order model (FOM) and the 56-state ROM, both with the 12 rigid body states removed, appear in Figure 4. As is evident from the figure, application of the B&T method gives a ROM that includes the important low-frequency structural modes, while neglecting the much higher frequency bending mode dynamics.

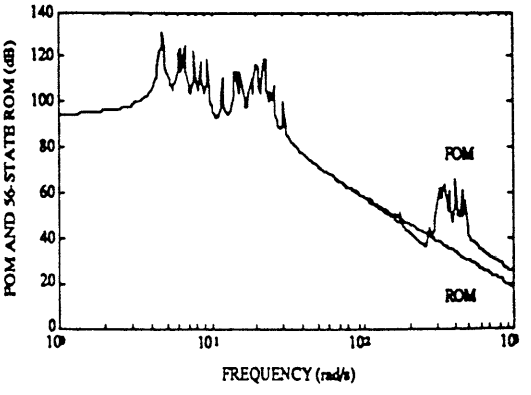

Figure 4. Full-Order and 56-State ROM Maximum Singular Value Frequency Responses.

4. A Framework for Robust Control System Design

Model reduction introduces errors into the design model that must be accounted for in system stability and performance analysis, and, hence, robust control

---

* Let G_k denote a k^{th} order ROM approximation to the plant, G. The absolute error is given by $\|G - G_k\|_\infty$, where $\|T\|_\infty$ indicates the H_∞-norm (or infinity-norm) of T (i.e., the maximum singular value of the transfer function, T, over all frequency).

techniques that ensure both stability and performance in the presence of modeling errors are required. For the SBL BEA segment phasing/jitter control problem, analysis with the well-known Small Gain Theorem (SGT) in combination with an appropriate controller design technique such as H_2 or H_∞ optimal control provides a suitable framework for robust control system design. Such a framework is convenient because it allows both stability robustness constraints and nominal performance conditions to be simply posed in terms of bounds on infinity-norms of certain transfer functions. Since the disturbance torques (and assumed measurement noise) provide the primary limitations on how small the segment phasing and LOS errors may be kept, nominal system performance can be characterized in terms of the frequency-dependent transfer from a combined disturbance vector, d, to a combined LOS and segment phasing error vector, e, while stability robustness may be guaranteed in terms of the following argument. For the system depicted in Figure 5, the Small Gain Theorem states that the nominally stable plant M(s) is stable for all stable perturbations $\Delta(s)$ if $\|M(s)\|_\infty \|\Delta(s)\|_\infty < 1$.

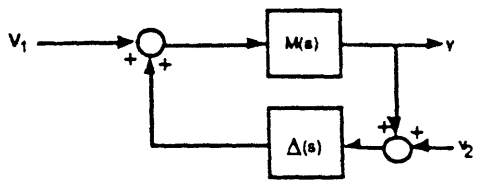

Figure 5. Topology for the Small Gain Theorem.

Consider Figure 6, where G(s) represents the open-loop plant ROM transfer matrix, $\Delta_M(s)$ is the error due to model reduction modeled as a multiplicative error at the plant output, u represents the actuator commands, and y includes the measured LOS and segment phasing errors. Further, assume without loss of generality that $\|\Delta_M(s)\|_\infty < 1$.* The block diagram of Figure 6 can be augmented to include the disturbance and performance signals, d and e respectively, as shown in Figure 7, and scaling may be performed so that the disturbance is RMS bounded by unity (i.e., $\sigma_d < 1$) and nominal performance specifications are met if $\sigma_e < 1$. Since the infinity-norm of a system transfer function bounds the ratio of the associated output/input RMS values, an H_∞ performance optimization problem may be constructed to minimize the infinity-norm of the closed-loop transfer from d to e, and if this quantity can be made less than 1 (implying nominal performance specifications are met), then stability robustness may be ensured via the SGT by verifying that $\|M(s)\|_\infty \|\Delta_M(s)\|_\infty < 1$.

* Scaling of Δ_m is easily incorporated into the plant by augmenting frequency-dependent weighting functions to the system matrices.

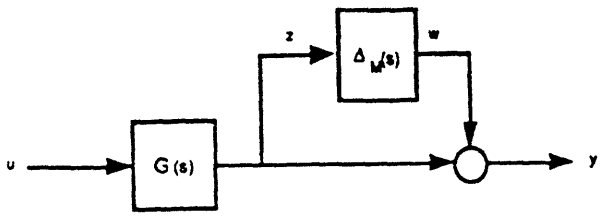

Figure 6. ROM with Modeling Error.

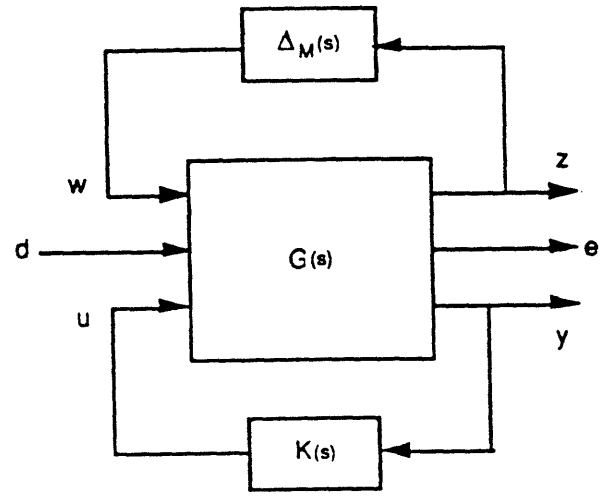

Figure 7. 3-Block Open-Loop Plant.

These nominal performance and stability robustness conditions may be restated more clearly by considering Figure 8, which illustrates the closed-loop transfer function from w and d to z and e, obtained from setting u = K(s)y.

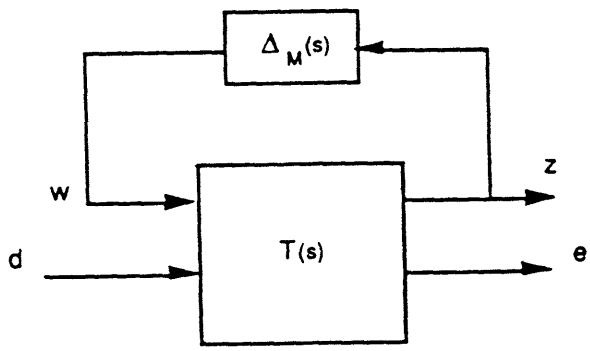

Figure 8. Closed-Loop Transfer Function.

Since the closed-loop transfer function, T(s), can be partitioned such that

$$\begin{bmatrix} z \\ e \end{bmatrix} = \begin{bmatrix} T_{11}(s) & T_{12}(s) \\ T_{21}(s) & T_{22}(s) \end{bmatrix} \begin{bmatrix} w \\ d \end{bmatrix}$$

then, in the context of the framework discussed above, nominal system performance specifications are met as long as

$$\|T_{22}(s)\|_\infty \leq 1$$

and stability robustness is ensured if

$$\|T_{11}(s)\|_\infty \leq 1$$

A two-Riccati equation algorithm[4], commonly referred to as γ-iteration, provides an efficient solution to the H_∞ optimization problem. Also, although performance objectives for the example problem considered have been posed as minimizing the infinity-norm of a certain transfer function, the design framework presented is compatible with other controller synthesis techniques such as H_2 optimal control, for which standard solution methods are well known. Additionally, another suitable compensator synthesis technique is H_∞ loop-shaping, which results from augmenting frequency-dependent weighting functions to the system errors and/or controls, and applying the γ-iteration procedure to the resulting augmented plant. Results of application of all three of these design methods to the BEA segment phasing/jitter control problem are presented in Section 5.

Before leaving this section, however, it should be mentioned that the framework for robust control system design presented here addresses only stability robustness issues, and allows no general provisions for testing the robustness of performance. Performance robustness, or the guaranteeing of system performance in the presence of uncertainty, is not specifically designed for in the example problem. Performance robustness of the final design selected is, however, independently assessed in Section 7 for certain known types of system errors.

5. Compensator Designs

Results of application of the various compensator synthesis techniques are now presented. Arbitrary bounds selected for the allowable RMS values of the disturbance torque, segment phasing, and LOS error vectors are 0.35 Newton-meters (N-m), 0.15 micrometers (μm), and 0.10 microradians (μrad) respectively. Insignificant sensor noise is assumed. For purposes of convenient comparison, only maximum singular value response plots of the T_{11} and T_{22} blocks of each design and associated compensators are shown. Note that the disturbance and error vectors have been scaled as described in Section 4 so that $\sigma_d, \sigma_e \leq 1$.

Figures 9 and 10 show open- and closed-loop transfer maximum singular value plots from d to e and about Δ_M, respectively, for unconstrained bandwidth H_2 and H_∞ optimal controller designs. These designs are said to be of unconstrained bandwidth because although both the H_2 and H_∞ optimal control algorithms require inclusion of some multiple of all the controls in the system error (performance) vector, for these designs that multiple was chosen to be very small. As can be seen from Figure 9, both controllers result in achieving nominal performance specifications (closed-loop transfer infinity-norm from d to e less than 1 (0 dB)), but the H_∞ response is flatter and has a smaller infinity-norm (5 dB less) than the H_2 design, indicating better worst-case disturbance rejection properties. From Figure 10 it is clear that both unconstrained bandwidth designs violate the stability robustness test of the SGT. This seems to be occurring due to high gain being injected by the controllers at high frequencies, where a large modeling error exists due to neglected high-frequency dynamics.

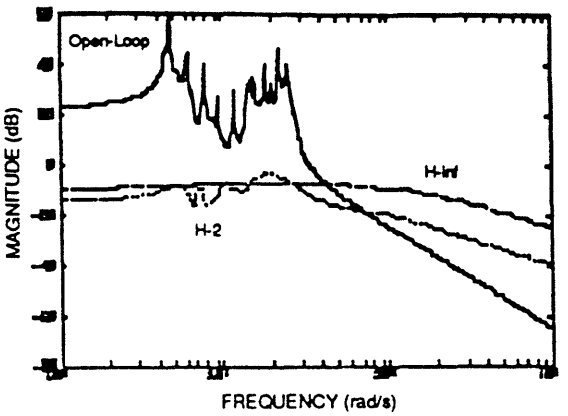

Figure 9. Open- and Closed-Loop Transfer from d to e.

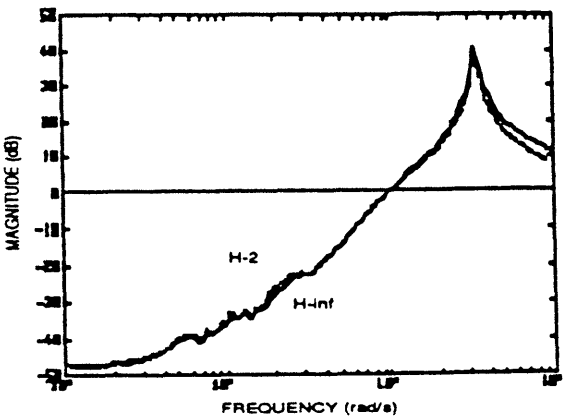

Figure 10. Closed-Loop Transfer About Δ_M (T_{11}).

To verify this, consider Figure 11, which shows the maximum singular value frequency responses of the unconstrained bandwidth H_2/H_∞ compensators. The high bandwidth nature of these compensators is obvious from the figure, as they can be seen to indeed inject very high gain at high frequencies, creating a possibility for excitation of the truncated bending mode dynamics, and leading to possible instability due to high-frequency gain considerations. Thus, from Figure 11 it is obvious why the unconstrained bandwidth closed-loop systems violate the stability robustness test of the Small Gain Theorem.

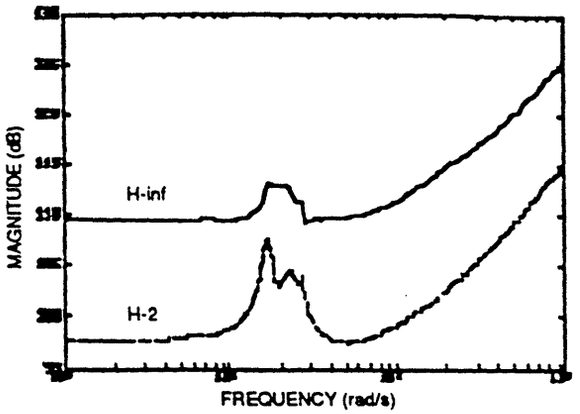

Figure 11. Unconstrained Bandwidth Compensator Maximum Singular Value Frequency Responses.

Traditional means of overcoming this high gain, high frequency problem involve increasing the constant multiple control penalty portion of the system error vector to a significant level. This tends to limit the amount of gain injected by the compensator at all frequencies so that the system bandwidth is decreased, which is desirable from a stability robustness point of view, but also has the undesirable consequence of degrading low-frequency performance. Stability robustness is obtained via this technique by increasing the penalty weighting on u until the gain injected at high frequencies diminishes enough to offset the large modeling error present.

Figures 12 and 13 show open- and closed-loop transfer maximum singular value plots from d to e and about Δ_M, respectively, for H_2 and H_∞ designs with an error vector that has been augmented with a suitably large control penalty term. The figures indicate that stability robustness is attained with both designs by frequency-independent penalization of u, but at a price of sacrificing about one order of magnitude (20 dB) in closed-loop d to e infinity-norm, so that nominal performance specifications are no longer met. Thus, although the constant control penalty reduced bandwidth designs are robustly stable to the truncated dynamics and do outperform the open-loop system, their disturbance rejection performance properties are unacceptable.

To gain more insight into how stability robustness has been achieved with these designs, consider Figure 14, which shows the maximum singular value frequency responses of the robust H_2 and H_∞ reduced bandwidth compensators. The most significant point to be observed from the figure is that now both compensators are rolling off the injected gain at a frequency of ~100 rad/s, which allows the designs to meet the stability robustness test of the Small Gain Theorem. Also important to note is the over two orders of magnitude

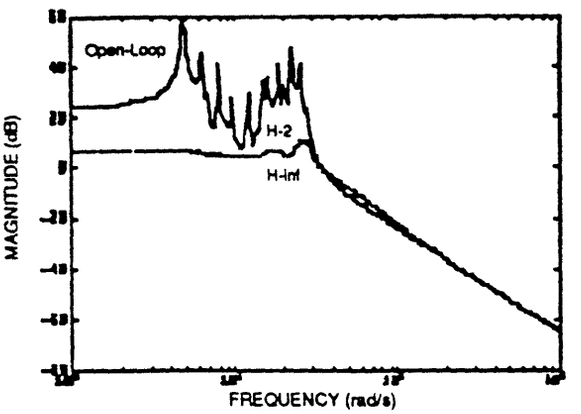

Figure 12. Open- and Closed-Loop Transfer From d to e (Controls Penalized).

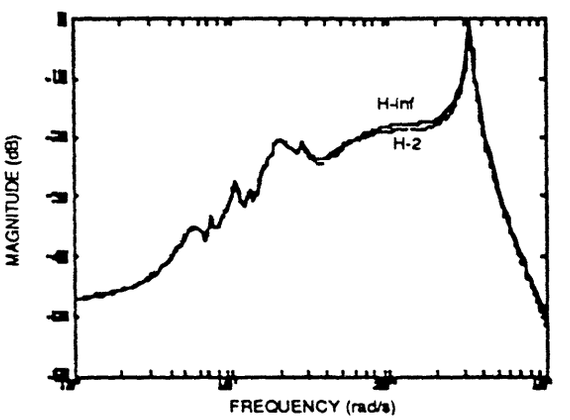

Figure 13. Closed-Loop Transfer About Δ_M (T_{11}) (Controls Penalized).

(40 dB) drop in gain injected at low frequencies as compared to the unconstrained bandwidth designs (reference Figure 11), resulting in the robust designs' observed degradation in nominal performance. This is the expected result of constant control penalty, which acts at low as well as at high frequency.

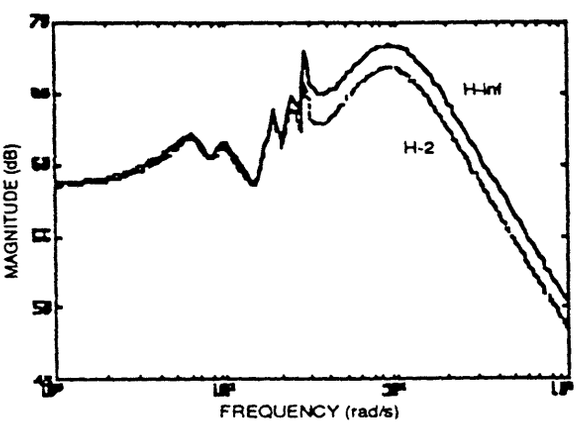

Figure 14. Robust Compensator Maximum Singular Value Frequency Responses.

From the results presented thus far, it can be seen that penalizing the system control at all frequencies proves effective in attaining closed-loop stability robustness, but results in an unacceptable degradation of system disturbance rejection performance, particularly at low frequencies. Alternate means of achieving stability robustness without greatly sacrificing achievable performance are therefore required. From Figures 11 and 14, it seems that what is needed is a methodology that induces the compensator to inject higher gain at low frequencies (thereby improving performance), while still forcing a fast roll-off of gain at high frequencies in order to meet the stability robustness constraint. This design objective suggests the use of frequency-dependent design techniques, otherwise known as loop-shaping methods.

As mentioned previously, the technique of H_∞ loop-shaping is carried out by augmenting frequency-dependent weighting functions to the system performance vector, and subsequent solution of the H_∞ Riccati equations in the γ-iteration process. For the problem at hand, the results shown thus far suggest that frequency-dependent penalty of the controls portion of the performance vector offers hope for an acceptable solution to be obtained. Penalizing the controls significantly more at high frequencies than at low frequencies should allow the design to inject high gain at low frequencies, thereby improving low-frequency disturbance rejection properties, while simultaneously forcing the compensator to roll-off the high-frequency gain so as to meet the stability robustness constraint. Such a design is now presented.

Consider Figure 15, which shows the singular value frequency response for a single-input/single-output control weighting function with a zero at s = -5 rad/s, a pole at s = -500 rad/s, and a dc gain of 77, selected to meet the above criteria and arrived at via trial and error iteration. Figures 16 and 17 show the closed-loop transfers from d to e and about Δ_M for the H_∞ loop-shaped design obtained by augmenting the dynamics of the above control weighting transfer function to every control channel of the open-loop model and solving the H_∞ Riccati equations. As can be seen from Figure 16, the maximum singular values of the T_{22} block are less than 1 (0 dB) at all frequencies, so that the H_∞ loop-shaped control design obtained meets nominal performance specifications. Similarly, Figure 17 indicates that the H_∞ loop-shaped control design is guaranteed to be robustly stable. Thus, this design is deemed acceptable.

Figure 18 shows the maximum singular value frequency response of the weighted-control H_∞ design compensator. The most significant difference between the frequency response of this compensator and the robust H_2/H_∞ compensator responses is the markedly

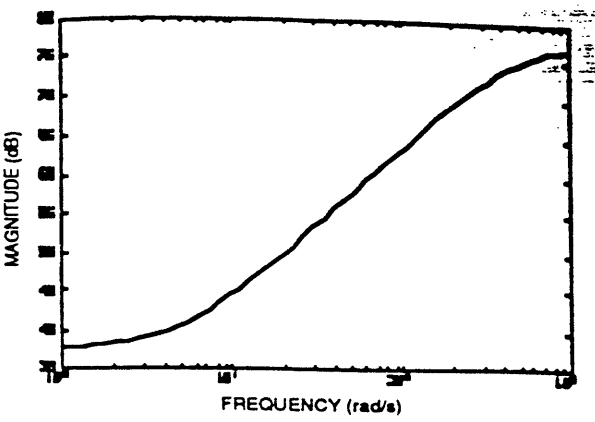

Figure 15. Control Shaping Filter Frequency Response.

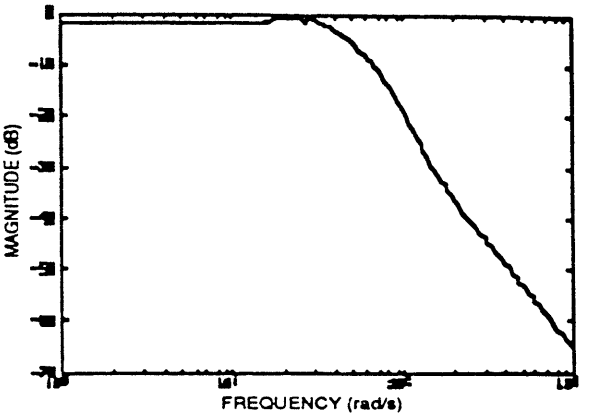

Figure 16. Closed-Loop Transfer from d to e (T_{22}) (Weighted-Control H_∞ Design).

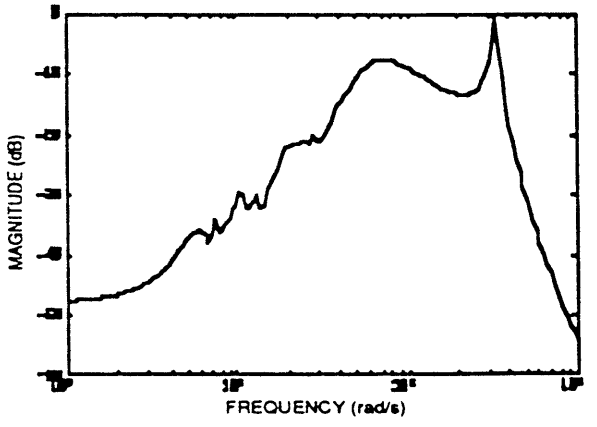

Figure 17. Closed-Loop Transfer about Δ_M (T_{11}) (Weighted-Control H_∞ Design).

higher gain maintained by the loop-shaped H_∞ compensator over the low-frequency region. This allows the H_∞ loop-shaped control compensator to meet performance specifications in the frequency range where the other designs do not. Further, it is the ability of the H_∞ loop-shaped control compensator to preserve high gain through ~100 rad/s and still roll-off fast enough to

meet the stability robustness constraint that is especially crucial to the success of this design. Finally, Figure 18 indicates that there is a region of particularly high compensator gain between ~18 and 30 rad/s, including what appears to be a very lightly-damped compensator pole at ~28 rad/s. The clear presence of this pole seems to indicate that the compensator is performing some type of critical pole-zero cancellation of the plant dynamics at ~28 rad/s, in order to extend the design's disturbance rejection capability to higher frequencies.

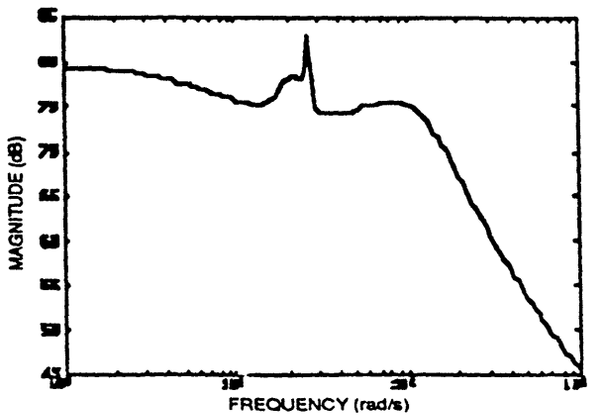

Figure 18. H_∞ Loop-Shaped Control Compensator Maximum Singular Values.

6. Design Simulation

In this section, the H_∞ loop-shaped control compensator obtained in Section 5 is validated via time domain simulation. Representative time responses are presented which illustrate characteristic system behavior under the influence of filtered white noise disturbances and demonstrate satisfaction of nominal performance specifications. Open- and closed-loop results are presented simultaneously in order to facilitate comparison between the two cases.

Since large-scale flexible space structures like the SBL envisioned here have yet to be built and tested, the time-domain nature and spectral properties of the torque disturbances and measurement noise present in the BEA system are not precisely known. Therefore, the assumption is made that the disturbances can be represented as random processes with typically broadband spectral characteristics and bounded RMS values. One convenient way of modeling such processes is to represent them as outputs of linear-time-invariant low-pass systems driven by white noise, otherwise known as colored noise processes. As long as the bandwidth of the coloring filter is selected to be greater than the bandwidth of the system being driven, colored noise inputs may be used to excite all system natural frequencies. Modeling the system disturbances as colored noises therefore allows the dominant frequency-dependent behavior of the system to be elicited.

Figures 19 and 20 show representative time responses of two BEA torque disturbances, generated by passing white noise through a simple first-order low pass filter with bandwidth just greater than the bandwidth of the loop-shaped H_∞ closed-loop system. The random nature of the torque disturbances is obvious from the plots, as any two consecutive values seem to be highly uncorrelated. The RMS values of the torque disturbances also seem to be accurately represented, as it appears that 95 percent of the values lie within the 3σ margins of $\pm$ 0.75 N-m (note that two individual torque RMS values of 0.25 N-m combine to yield the chosen 0.35 N-m torque vector RMS value).

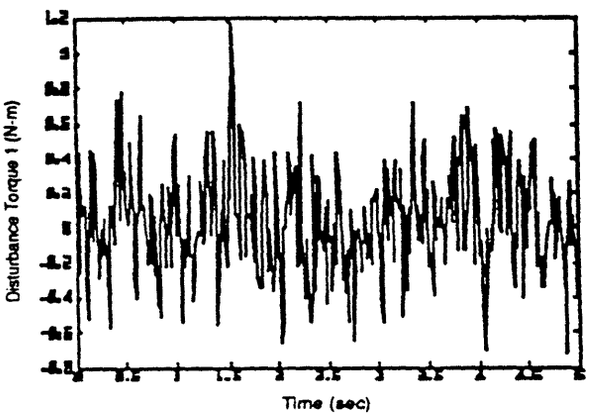

Figure 19. Torque Disturbance 1 Time Response.

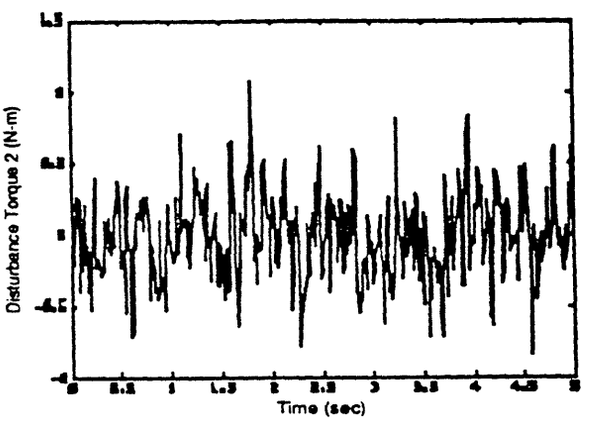

Figure 20. Torque Disturbance 2 Time Response.

Figures 21 and 22 respectively show the open- and closed-loop segment phasing errors at measurement position 4 (reference Figure 2) resulting from application of the disturbance torques of Figures 19 and 20. From the figures, it can be seen that, on the average, the open-loop response is significantly larger than the closed-loop response, as expected. In fact, the largest amplitude of the open-loop error is more than twenty times the magnitude of the largest closed-loop error amplitude, indicating a significant improvement in performance between the closed and open-loop systems. The open-loop error also appears in general to be less

jagged than its closed-loop counterpart, or in general more slowly time varying. This can be interpreted as meaning that the open-loop error is dominated by low-frequency components, while the closed-loop error is dominated by higher-frequency components. Since the compensator employed in the closed-loop system was designed specifically to reject low-frequency disturbances, this interpretation makes sense. Also note that both these error time responses are significantly less jagged than the torque disturbances. This effect can be attributed to the high-frequency attenuation resulting from passing the colored-noise disturbances through a lower-bandwidth system. As a final remark, note that a rough estimate of the closed-loop RMS position 4 segment phasing error of 0.02 μm projected into a 6 element segment phasing vector yields a total RMS value of 0.05 μm. Since this value is significantly less than the specified segment phasing performance bound of 0.15 μm, it appears that the H_∞ loop-shaped control design can indeed be seen to meet nominal performance specifications.

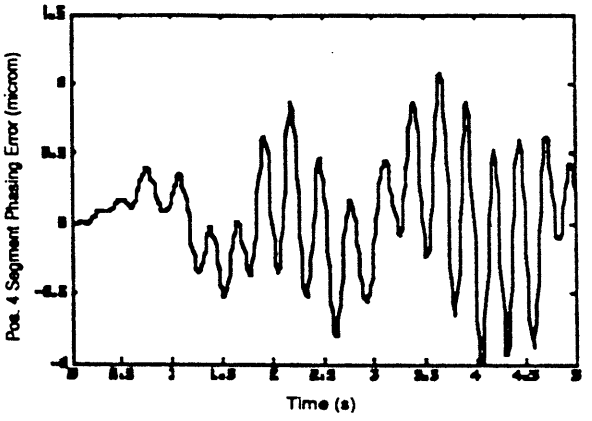

Figure 21. Open-Loop Position 4 Segment Phasing Error Time Response.

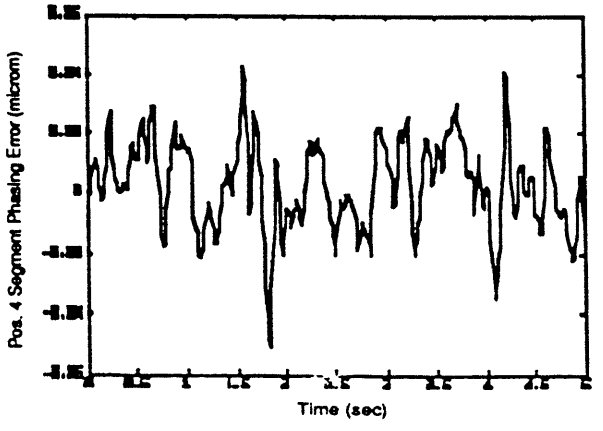

Figure 22. Closed-Loop Position 4 Segment Phasing Error Time Response.

7. Performance Robustness and Effects of Open-Loop Pole Parametric Uncertainty

It is well-known that optimal controllers alter the behavior of the open-loop plant via the mechanism of "approximate plant inversion", in which undesirable system poles and zeros are respectively cancelled with compensator zeros and poles, and the best system response achievable is then obtained via selection of any additional compensator pole/zero locations. One obvious flaw in such a design methodology is that uncertainty invariably exists in the location of the open-loop poles, due to approximations and errors in the modeling process. If the true system poles are not exactly the same as those of the design model, then the multivariable pole-zero cancellations employed by plant-inverting techniques are not likely to be completely successful, and may even lead to serious degradations in nominal system stability and performance. It is thus of interest to the designer to somehow assess the potential impact of open-loop pole location errors prior to compensator implementation. Therefore, in this section it is demonstrated how the Small Gain Theorem may be used to assess the stability robustness of the weighted-control H_∞ loop-shaped compensator closed-loop system to five percent parametric uncertainty in the open-loop finite-element model stiffness matrix elements, corresponding to two and one-half percent parametric uncertainty in the open-loop natural frequencies. Since the Small Gain Theorem is known to be conservative, the actual effects of open-loop pole location errors on closed-loop stability for two specific perturbed natural frequency models is then directly verified via computation of the closed-loop poles. Finally, robustness of performance of non-perturbed and perturbed models is assessed via computation of closed-loop d to e transfer function frequency responses.

As discussed in Section 5, the Small Gain Theorem may be used to conservatively assess the stability robustness of any system containing uncertainty, as long as that uncertainty may be gain-bounded as a function of frequency. In particular, a framework has been developed for testing the stability robustness of systems where the only uncertainty in the plant is modeled as a multiplicative error at the plant output. As was previously developed, stability robustness of such an uncertain system may be guaranteed by ensuring that the infinity-norm of the closed-loop transfer about the uncertainty block, $\|T_{11}(s)\|_\infty$, is less than one, as long as the infinity-norm of the uncertainty block is unity bounded. Consider Figure 23, which shows the maximum singular value frequency responses of multiplicative errors, $\Delta_M(s)$, at the plant output for two perturbed natural frequency systems, and of a transfer function which effectively bounds both the errors. As can be seen from Figure 23, the nominal design model possesses large errors at high-frequency due to model-reduction truncation of the high-frequency modes (as was previously the case for the unperturbed system), but now there is also significant error at low frequency due to the difference between modeled and "actual" open-loop natural frequencies.

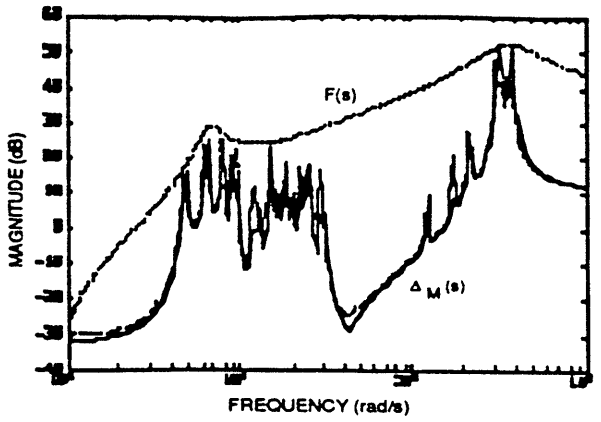

Figure 23. Perturbed System Multiplicative Errors at the Plant Output and Bounding Transfer Function Frequency Responses.

Figure 24 shows the closed-loop transfer maximum singular values about the delta block for the perturbed plant models. As can clearly be seen from the figure, the maximum singular values of the closed-loop transfer about the uncertainty block exceed unity (0 dB) over almost all of the frequency range of interest. Figure 24 therefore indicates that the closed-loop system is not guaranteed to be robustly stable to two and one-half percent error in open-loop natural frequencies according to the sufficient test of the Small Gain Theorem. The Small Gain Theorem is based purely on gain considerations, however, and is known to be conservative. Therefore, the actual closed-loop systems

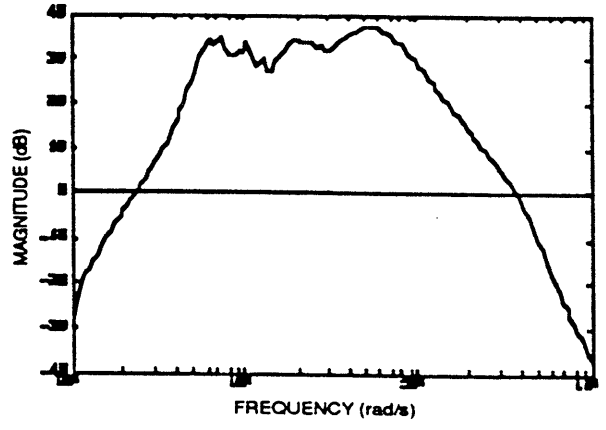

Figure 24. Closed-Loop Transfer about Δ_M (T_{11}) (Perturbed Open-Loop Natural Frequency Systems).

using the perturbed natural frequency models and weighted-control H_∞ loop-shaped compensator may be formed, and the closed-loop poles and d to e transfer function maximum singular value frequency responses computed to verify the actual effects of the parametric uncertainty. In doing this for the two perturbed open-loop models chosen, the resulting closed-loop systems are found to be stable, in spite of the indications of the stability robustness test of the Small Gain Theorem. The conservatism of the SGT is thus made apparent. Severe degradations in closed-loop performance do however result, as can be seen from Figures 25 and 26 below, which show the maximum singular value closed-loop d to e transfers for the systems with respectively five percent greater and less stiffness than the original model. The figures clearly illustrate the importance of feeding the precise location of the open-loop poles and zeros to the optimal control problem. Note that even in the presence of open-loop natural frequency parametric uncertainty, closed-loop performance specifications are met at low frequency, and the degraded higher frequency performance is, in general, still superior to that of the open-loop system.

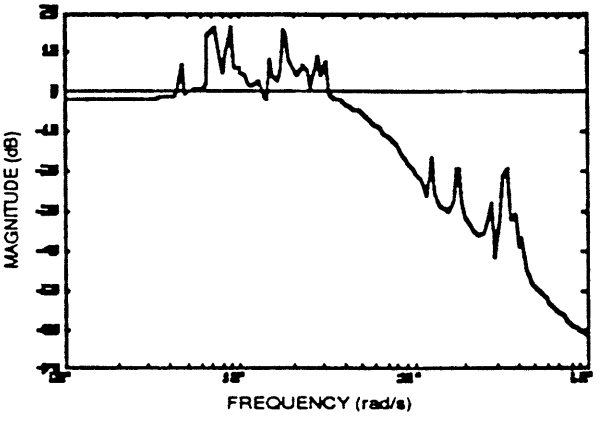

Figure 25. Closed-Loop Transfer from d to e (T_{22}) (5% More Stiff Open-Loop System).

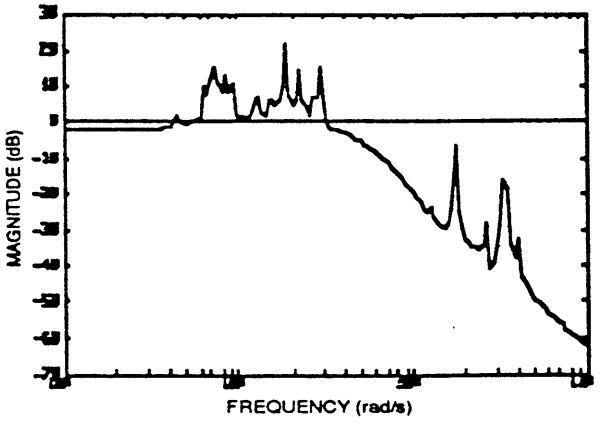

Figure 26. Closed-Loop Transfer from d to e (T_{22}) (5% Less Stiff Open-Loop System).

Since performance specifications are not met in the presence of two and one-half percent open-loop natural frequency parametric uncertainty, the closed-loop system does not possess robustness of performance to these types of structured parameter errors. This observation raises the question of whether or not the closed-loop system displays robustness of performance to the errors due to truncation of modes brought about by model

reduction. To answer this question, consider Figure 27, which shows the closed-loop frequency response from d to e for the full-order model with no parametric uncertainty. As can be seen from the figure, the system does indeed possess robust performance for the errors due to model reduction.

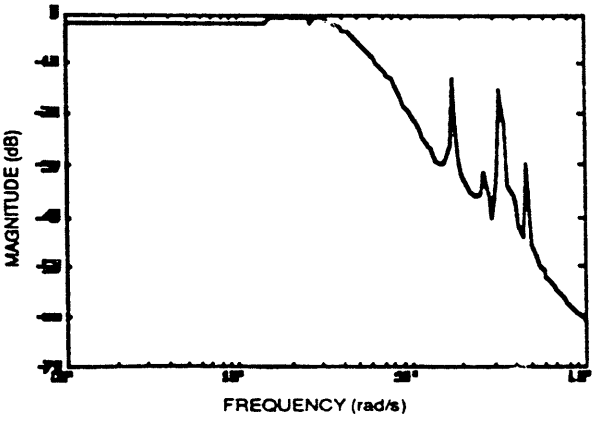

Figure 27. Closed-Loop Transfer from d to e (T_{22}) (Full-Order Open-Loop System).

8. Conclusions

In this paper, the utility of applying optimal controller synthesis methodologies in conjunction with model reduction techniques and the stability robustness test of the Small Gain Theorem to robust control of large-scale systems has been demonstrated, and several interesting consequences of adopting this design approach have been illustrated. Controller design for large-scale systems necessitates reduction of model order, and in this paper ideally performing but unconstrained bandwidth designs were developed for a space-based laser example problem to illustrate the dangers of totally ignoring the effects of the resulting unmodeled dynamics. In particular, the Small Gain Theorem was used to show the strong possibility of closed-loop instability for these designs. Reduction of closed-loop bandwidth via constant control penalty was seen to achieve guaranteed stability robustness, but at an unacceptable cost of large sacrifices in performance. The added degrees-of-freedom afforded by H_∞ loop-shaping techniques were then used to overcome this problem, resulting in a design meeting both robust stability and nominal performance conditions. However, severe degradations in performance were seen to result from parametric uncertainty in open-loop pole/zero locations, illustrating the fact that one should not realistically expect ideal performance in a practical setting. Finally, although it had not been specifically designed for, the H_∞ loop-shaping design was seen to possess performance robustness to the dynamics removed in the model reduction process.

9. References

1. Flueckiger, K., Dowdle, J. and Henderson, T., "A Control System Design Methodology for Large-Scale Interconnected Systems", *Proceedings of the 1990 American Control Conference*, San Diego, CA, pp.428-434.

2. Hammett, K., Dowdle, J., Athans, M., and Flueckiger, K., "Robust Control System Synthesis for Space-Based Laser Beam Control", to appear *Proceedings of the 1991 American Control Conference*, Boston, MA.

3. Moore, B.C., "Principle Component Analysis in Linear Systems: Controllability, Observability and Model Reduction," *IEEE Trans. on Auto. Control*, Vol. AC-26, pp. 17-32, 1981.

4. Glover, K. and Doyle, J., "State-Space Formulae for All Stabilizing Controllers that Satisfy an H_∞-norm Bound and Relations to Risk Sensitivity," *Systems & Control Letters*, 11 (1988) 167-172, North-Holland.